

Semi-Submersible Wind Turbine Hull Shape Design for a Favorable System Response Behavior

Frank Lemmer, Wei Yu, Kolja Mller¹, Po Wen Cheng

University of Stuttgart (SWE), Allmandring 5B, 70569 Stuttgart, Germany

Abstract

Floating offshore wind turbines are a novel technology, which has reached, with the first wind farm in operation, an advanced state of development. The question of how floating wind systems can be optimized to operate smoothly in harsh wind and wave conditions is the subject of the present work. An integrated optimization was conducted, where the hull shape of a semi-submersible, as well as the wind turbine controller were varied with the goal of finding a cost-efficient design, which does not respond to wind and wave excitations, resulting in small structural fatigue and extreme loads.

The optimum design was found to have a remarkably low tower-base fatigue load response and small rotor fore-aft amplitudes. Further investigations showed that the reason for the good dynamic behavior is a particularly favorable response to first-order wave loads: The floating wind turbine rotates in pitch-direction about a point close to the rotor hub and the rotor fore-aft motion is almost unaffected by the wave excitation. As a result, the power production and the blade loads are not influenced by the waves. A comparable effect was so far known for Tension Leg Platforms but not for semi-submersible wind turbines. The methodology builds on a low-order simulation model, coupled to a parametric panel code model, a detailed viscous drag model and an individually tuned blade pitch controller. The results are confirmed by the higher-fidelity model FAST. A new indicator to express the optimal behavior through a single design criterion has been developed.

Keywords: Floating wind turbine, Integrated design, Wave cancellation, Counter-phase pitch response, Systems Engineering
2010 MSC: 00-01, 99-00

1. Introduction

First concept and feasibility studies for Floating Offshore Wind Turbines (FOWTs) appeared more than 15 years ago [1]. Since then, prototypes of

Email address: lemmer@ifb.uni-stuttgart.de (Frank Lemmer)

¹Independent researcher

spars, semi-submersibles, barges and Tension Leg Platforms (TLPs) have been built [2]. The present paper aims at particular design indicators for semi-submersibles for a favorable response behavior in wind and waves. The next sections will first provide an introduction of the inherent FOWT dynamic characteristics followed by a review of published design procedures.

1.1. System dynamics of floating wind turbines

The commonly employed dynamic aero-hydro-elastic models for FOWTs involve assumptions comparable to the FAST model by National Renewable Energy Laboratory, Boulder, USA (NREL) [3]. This open-source tool is used as a reference model in the present work.

Most models employ elastic Multibody Systems (MBSs) of reduced order through an approximation of the tower and blade deformation with a superposition of their respective mode shapes. FAST has in this work 25 enabled Degrees of Freedom (DoFs). The low-order model, on the other hand, has six DoFs, covering only the 2D planar motion of the system. The term “low-order” refers in this work to the number of DoFs of the dynamic equations of motion. Coupled dynamic models consider, next to the elastic forces, centrifugal, gyroscopic and Coriolis forces, which are significant for systems of large rigid-body motions. The coupling effects are important for the system dynamics, because the elastic body mode shapes vary when coupled into a multibody system. An example is the coupling of the tower flexibility with the floater rigid body modes or the controller closed-loop dynamics with the fore-aft mode.

The wind turbine blade pitch controller is especially critical for FOWTs: A standard rotor-speed controller for above-rated wind speeds will pitch the blades when the rotor speed exceeds its rated value. In the case of FOWTs, this feedback loop can imply, as a side-effect, that the tower or the platform experiences large excursions, due to the aerodynamic properties of the rotor. When the relative wind speed (the one seen by the rotor) increases, the controller will pitch the blades towards feather (increasing blade pitch angle) and thereby reduce the aerodynamic rotor torque. As a consequence, the thrust also decreases. This means, on the other hand, that an oscillation of the platform in pitch will become unstable if the controller reacts sufficiently fast to the sinusoidally oscillating relative wind speed, see [4, 5].

External excitations arise from wind and waves. The wind turbulence excites the low-frequency platform modes as well as the blades and the tower-top at multiples of the rotor rotational frequencies. Dynamic effects due to the fore-aft motion of the rotor, accelerating the bulk flow across the turbine are subject to current research, i.e. [6, 7, 8]. Hydrodynamic forces, important for the system dynamics of semi-submersibles, are the Froude-Krylov wave loads including diffraction, viscous drag excitation, viscous drag damping (both from Morison’s drag term) [9, 10, 11] and second-order slow-drift forces at the difference-frequency of bichromatic waves from potential flow theory, i.e. [12, 13]. The first-order wave force coefficient can feature an attenuation range for semi-submersibles, also called the “wave cancellation effect”, see [14] and [15, p. 290].

For a representation of the overall FOWT response, the mooring line dynamics might be of negligible influence in the case of catenary mooring lines [16, 17].

1.2. Floating wind turbine design

Several schemes for the sequential design of FOWTs have been published in [18, 19, 20, 21, 22]. The report of the European project LIFES50+² [23] provides a comprehensive literature review of the FOWT design process and summarizes the findings in a consolidated scheme consisting of three stages. This work does not introduce a new design procedure, but a favorable effect that becomes visible in an integrated simulation study, covering a range of system parameters. In order to understand the existing constraints and barriers for an integrated design procedure, these are outlined in this section, before addressing the present design and simulation methodology.

Commonly, the design of a floating platform starts with static calculations, the so-called spreadsheet design phase. In this phase, the main dimensions of the structure can be determined, satisfying the requirement of hydrostatic restoring with an approximate structural dimensioning. It includes also frequency-domain analyses of the floater rigid body and the mooring lines. The first stage terminates with first experiments and an approximation of the expected cost of energy. In the subsequent stage, the first coupled dynamic simulations take place, which require a wind turbine model and a controller.

The manifold of design constraints of a FOWT are represented in various standards and guidelines [24]. Published design studies have addressed the structural integrity, dynamic behavior, manufacturing, installation and marine operations, among others. An academic concept design study across different platform types was presented in [25], outlining the main assumptions and design constraints. A spar platform out of concrete was designed, simulated and tested in [26, 27]. The constraints and options for manufacturing of that design are discussed and summarized in [28]. A comparable design of reduced draft was presented in [29] with a focus on seakeeping of the floater and marine operations. The peculiar loads of a steel semi-submersible with submerged counter-weight are calculated in [30] with a focus on the cables, sustaining the counter-weight. A semi-submersible for a very large wind turbine was recently presented in [22].

Further studies focused on methods for obtaining the structural stresses of the floater in extreme and fatigue load cases. One of the first approaches was presented for a steel semi-submersible in [31]. The difficulty of obtaining the structural loads is due to the fact that most available coupled simulation codes assume the floater is rigid, which makes it impossible to calculate internal stresses. Ways to overcome this limitation were presented in [32, 33, 34, 35]. These methods involve either additional DoFs of the dynamic model or additional engineering steps in decoupled analyses. Often, the tower-base bending moment, which is available in standard simulation models, is taken as repre-

²<http://www.lifes50plus.eu>, accessed on July 18, 2018.

sentative structural load in optimization studies. It is influenced by both, wind and wave loads.

First integrated optimization studies for TLPs and spars were presented in [36]. A coupled frequency-domain model was used to calculate the tower-top acceleration for various shapes of the floating platform and different slack and taught mooring configurations. Later, optimization studies on spar platforms were presented [37], including load calculations and a cost model. An adaptation of the wind turbine controller was first included using the same simulation model as in the present work in [38, 39].

A large optimization study across different platform types was published in [40] and later extended in [41]. It includes the hull shape and mooring line design and a genetic optimizer. In that work, a frequency-domain model is derived from the code FAST [3], with a linear representation of the hydrodynamic viscous damping but without representing the wind turbine controller. The objective was also here a low nacelle acceleration, next to the estimated cost. The objective of the present work, as well as the design and simulation methodology will be outlined in the next section.

1.3. Parametric design and simulation approach

The methodology of the present work builds on parametric design routines (i.e. estimating steel thicknesses for structural integrity) on the one hand and parametric simulation models on the other hand. The design task in this paper considers a variation of the hull shape of a three-column concrete semi-submersible with varying draft and the wind turbine controller.

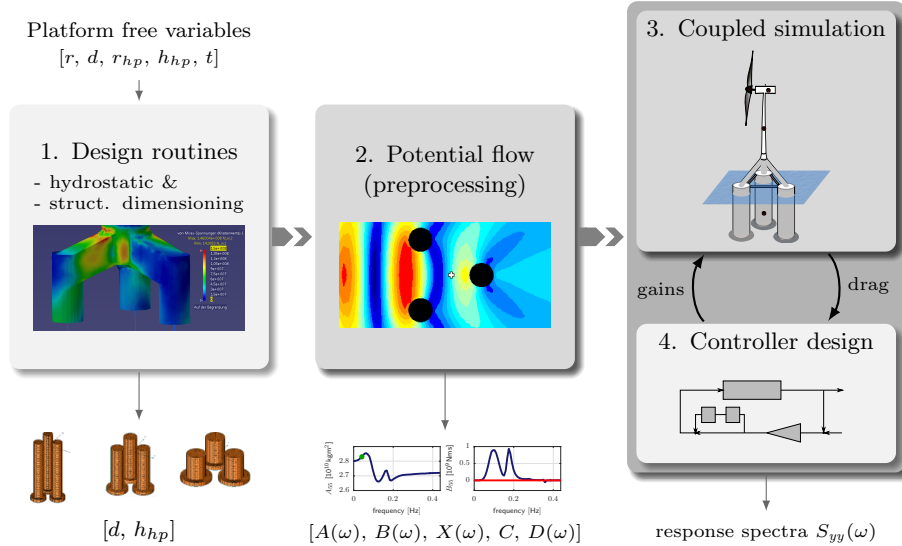


Figure 1: Parametric FOWT system design and brute force optimization scheme.

Figure 1 shows the main steps: The initial free variables parameterize the hull shape. As a function of these, a reasonable design space will be defined, with only few free variables to clearly visualize, interpret and understand the results, as shown in the next section. Based on this initial design space, the spreadsheet design routines ensure that each design satisfies basic constraints, related to the structural dimensions and the hydrostatic restoring, which is subject of Section 3. The result of this step is a design space of only two dimensions. The designs range from a slender, deep-drafted semi-submersible to a design of large breadth, large column radius and shallow draft. All designs are three-column semi-submersibles with heave plates. Hence, no discontinuities are present.

An adapted low-order aero-hydro-servo-elastic simulation model will be used for the analysis, as introduced in Section 4. It includes all effects relevant for the main system dynamics, which are sought to be optimized. Therefore, effects like the floater structural elasticity or advanced aerodynamic effects are not considered. For all shapes, the first-order hydrodynamic coefficients are calculated through a parameterized panel code model. These coefficients are input to the low-order model. The model includes Newman’s approximation to account for second-order slow-drift forcing. It includes also member-based viscous drag coefficients. The model is described in detail in [42, 43].

The viscous heave plate drag model is rather detailed because it influences the fore-aft motion and the coupling with the controller. The vertical heave plate drag coefficients are parameterized as a function of the Keulegan-Carpenter number $KC = vT/D$, which depends on the significant member length D , the response velocity magnitude v and its period T .

The wind turbine blade-pitch controller design routine is a function of a linear state-space model, including the viscous drag coefficients. For this reason, the system response has to be solved for iteratively because the controller depends on the drag coefficients, which in turn depend on the response magnitude. Examples for the analyzed results of Section 5 are the fatigue and extreme loads under realistic loading conditions, the modal properties and the harmonic response behavior to wind and waves.

The results of Section 6 will analyze and visualize the distinct dynamic properties across the design space. This analysis helps to understand the effects, which drive load and power fluctuations. From the findings, a new design objective is derived, extending the one of the nacelle acceleration used in previous works. The objective is focused on the dynamic system response while the component design is out of the scope of this paper.

2. Design Space

The selected hull shape parameters include the column spacing from the platform centerline d , the column radius r , the heave plate height h_{hp} , the ratio of heave plate radius to column radius $\hat{r}_{hp} = r_{hp}/r$ and the draft t , see Figure 2.

The column radius r is defined to be 52% of the maximum possible column radius $\hat{r}_{max} = d\sqrt{3}/2$ at which the three columns would touch each other. The

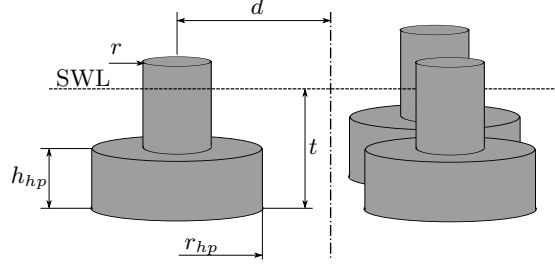


Figure 2: Free variables for parametric hull shape design, [43].

heave plate-to-column radius ratio is intended to be $\hat{r}_{hp,in}=2$ for all designs in order to ensure that the heave plates are large enough to effectively alter vertical added mass and Froude-Krylov forces. The heave plate-to-column radius ratio is altered, however, for the designs where the heave plates of the different columns would get too close to each other through an exponential function

$$\hat{r}_{hp} = r_{hp}/r = (r_{max}(d) - 1)(1 - \exp\left(\frac{\hat{r}_{hp,in} - 1}{\hat{r}_{max} - 1}\right)) + 1. \quad (1)$$

This ensures that no designs with unrealistically large heave plates result, which might not be manufacturable. The distance between overall center of mass and metacenter GM , i.e. [11], determines the restoring as

$$C_{55} = \rho g \nabla GM, \quad (2)$$

with the displaced volume ∇ of density ρ and the gravity constant g . Ballasting is such that zero trim is achieved. Thus, for given column diameters, a required C_{55}^* can be obtained by increasing the draft t , which lowers the center of gravity more than it raises the center of buoyancy and therefore increases C_{55} .

An upper draft limit of 80 m was considered in the a-priori definition of the bounds of the free variables. Hence, any shape considered in this study can be described by the two free variables column spacing d and heave plate height h_{hp} . This means that the design space (of the free variables) is Cartesian and the range of every variable does not depend on the values of the others. The small design space of feasible platforms makes a visualization and thorough analysis of the results possible. Table 1 lists the free variables and the dependent variables.

The semi-submersible main dimensions of the 2D design space are shown in Figure 3 with a column spacing range $d = 15.0(1.0)24.0$ m and a heave plate height range $h_{hp} = 1.0(3.5)8.0$ m. The designs range from slender, rather ballast-stabilized towards buoyancy-stabilized shallow-drafted semi-submersibles. Larger column spacings than the ones considered are expected to result in excessive bending stresses in the tripod structure. The variable heave plate height has the main effect of modifying the vertical Froude-Krylov forcing. Thus, this variable may be able to facilitate the above-mentioned wave cancellation effect. The images on top of Figure 3 show that the column radius is largest for the

Table 1: FOWT hull shape design parameters [43].

Free variables	Dependent variables
<ul style="list-style-type: none"> • Column spacing d • Heave plate height h_{hp} 	<ul style="list-style-type: none"> • Column radius r • Heave plate radius r_{hp} • Draft t • Steel tripod strut width & sheet thickness • Ballast mass • Platform mass distribution • Mooring line fairleads position • Wind turbine controller gains

lowest draft. The cost increases generally for increasing column radii r but decreases for the buoyancy-stabilized ones of shallow draft. The assumptions for the material cost estimation will be given in Section 3, it is roughly proportional to the submerged volume. The three designs shown in Figure 3 will be selected in a number of the upcoming analyses and indicated by “deep draft”, “medium draft”, and “shallow draft”.

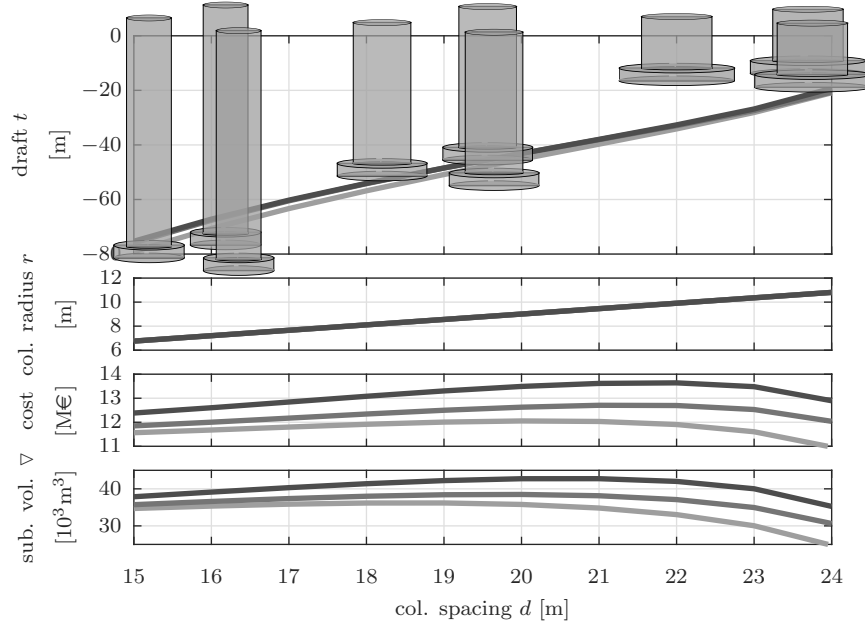


Figure 3: Design space with two dimensions: column spacing from centerline and heave plate height. Heave plate height $h_{hp} = [1.0, 4.5, 8.0]$ m (increasing darkness), [43].

3. Parametric Design Routines

This section addresses the design routines, which determine the dependent variables of Table 1. It starts with the structural design of the concrete floater with the steel tripod on top, followed by the mooring lines and the tower. Hydrostatic computations and the panel code calculations follow thereafter in Sections 3.2–3.3. The wind turbine controller is also parameterized and subject of Section 3.4. The wind turbine design, used for all platforms, is the DTU 10 MW Reference Wind Turbine (RWT) of [44].

3.1. Structural design

Design routines, which were developed for the concrete columns, the heave plates and the steel tripod will be described in this section. The result of the structural design calculation is mainly the mass distribution, next to the shape of the hull, which will be input to the coupled simulation model. The assumed material properties, costs and wall thicknesses of the columns are listed in Table 2, based on [45].

Table 2: Structural design assumptions, [43].

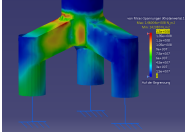
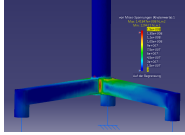
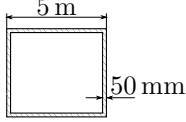
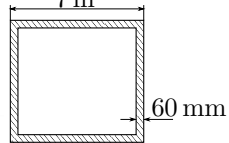
Parameter	Unit	Value
Reinforced concrete average density	[kg/m ³]	2750.0
Steel density	[kg/m ³]	7750.0
Ballast density	[kg/m ³]	2500.0
Processed steel cost	[€/t]	4500
Processed concrete cost	[€/t]	399
Concrete column wall thickness	[m]	0.6
Heave plate upper and lower lid thickness	[m]	0.4

3.1.1. Steel tripod

For the steel tripod, various Finite Element (FE) analyses were performed, covering the range of radial distances of the columns d as shown in Figure 3. The results of these calculations allow a parameterization of the dimensions of the steel legs like the sheet metal thickness, the strut width and height. The calculations assume a static thrust force at the tower-top of 4605 kN, as given in [44, p. 61]. The notch stress at the joint between the tower and the tripod struts is assumed to be the critical failure mode. The dimensions of the struts are determined such that the maximum notch stress is of comparable magnitude as the one resulting from the same calculation with a comparable commercial tripile. The method was first applied in the European project INNWIND.EU³, of which details can be found in [46]. The dimensions of the tripod of the minimum and maximum column spacing are shown in Table 3.

³<http://www.innwind.eu>, accessed on July 18, 2018.

Table 3: Parametric design of the TripleSpar steel tripod, [43].

	Min. column spacing	Max. column spacing
		
		
Column spacing (distance to center)	10.0 m	35.0 m
Strut width & height	5.0 m	7.0 m
Steel wall thickness	50 mm	60 mm
Maximum stress	146.0 N/mm ²	142.0 N/mm ²
Tripod mass	447 t	1716 t

3.1.2. Concrete columns and heave plates

The concrete columns are of pre-stressed concrete following the example of the AFOSP spar design, see [26]. The cylindric walls have a constant thickness for all of the hull shape variations, see Table 2. The heave plates are made out of reinforced concrete with the material properties given in Table 2. The heave plates are concrete rings, flush mounted to the lower ends of the columns. This assumption is rather conservative and accounts for further compartmentation and reinforcements of the detailed design phase.

3.1.3. Mooring lines

The properties of the mooring system can be found in [45]. It was designed for the TripleSpar design [45, 47], with two upwind lines and one downwind line with fairleads above Still Water Level (SWL), at $z_{frlds} = 8.7$ m and a radial distance from the tower centerline of $d_{frlds} = 26$ m. This large distance makes it possible to keep the same mooring system for all column spacings d of Figure 3.

3.1.4. Tower

The tower design is not varied in the optimization study but the parameters of the reference TripleSpar are used [45]. For FOWTs it is important that the tower eigenfrequency does not coincide with the Three-Times-Per-Revolution (3p)-frequency range of the rotor. However, the considered platforms of Figure 3 show only little variations of the eigenfrequencies. This is mainly due to the hydrostatic design constraints (Section 3.2). Consequently, no adaptation of the tower design is considered in this work.

3.1.5. Cost estimation

FOWT cost models have been subject of different research projects with a good overview and summary in [48, 49]. For this work, a cost of the processed material of the concrete heave plates and columns and the steel tripod, including both, material and manufacturing costs, is assumed. The values are in line with LIFES50+ Deliverable 4.3 [50] and can be found in Table 2. The cost levels shown in Figure 3 are comparable to the ones of [49]. Other costs than the ones mentioned, like installation, assembly and O&M costs are not considered. It is noted that these values are rough approximations, which might change due to concrete shrinkage and also due to existing price fluctuations over time.

3.2. Hydrostatic design

The hydrostatic restoring stiffness in pitch-direction C_{55} is a driving property, which influences the FOWT mean pitch angle under wind loads and therefore the power losses from misalignment, the maximum amplitudes and the eigenfrequencies. In other works, such as [40], the value of C_{55} is free to vary in the design space and constraints on the pitch eigenfrequency are imposed.

In this work, the hydrostatic restoring was constrained, following the perception that the hydrostatic restoring is crucial for the above-mentioned FOWT properties. A variation of C_{55} might result in small changes in cost and performance, while a large change of its value is unrealistic. The restoring $C_{55} = 2.255 \times 10^9 \text{ Nm/rad}$ is set as constraint for all geometries of the design space. Depending on the free variables column spacing d and heave plate height h_{hp} , the draft, as remaining variable, is determined such that this constraint is satisfied. A root-finding algorithm, connected to the structural design and the hydrostatic functions, solves this problem. The steady state pitch angle is about $\beta_{p, \text{rated}} \approx 3.0 \text{ deg}$ at rated wind speed. It would change as a function of the fairlead vertical position, due to a different lever arm of the rotor thrust force. This vertical position, however, is constant throughout the design space.

3.3. Hydrodynamic coefficients

A parameterized panel model has been set up to calculate the hydrodynamic coefficients with Ansys Aqwa-Line.

The column drag coefficient is kept constant for all designs and sea-states. It has been selected conservatively as $C_D = 0.4$. In the case of the heave plates, the drag coefficient is iterated based on the experimental data given in [51]. This data was parameterized as a function of KC , which is possible because the Reynolds number and the surface roughness have little influence for shapes of sharp edges. For all designs, the vertical drag force is applied only at the lower (keel) surface of the heave plates and the bottom cross-sectional area of the heave plates is used for the calculation of the drag force. The iterative procedure is subject of the paper [52].

3.4. Controller design

As introduced in Section 1, the blade pitch controller of the wind turbine for above-rated wind speeds is critical for the FOWT system stability. In order to ensure a properly tuned controller for each of the designs of Figure 3, a method was developed to automate the design of a Single-Input-Single-Output (SISO) Proportional-Integral (PI)-controller, depending on the linear dynamic model. This model will be introduced in Section 4. The controller design procedure is subject of the companion paper [53] and part of the thesis [43], which includes a comparison against a multivariable controller.

Figure 1 of Section 1 shows on the right the iterative solution procedure to obtain the controller gains: It follows from the implementation of [52], which considers viscous drag coefficients of the heave plates that are a function of the KC -number, which is itself a function of the nodal response magnitude. The resulting platform viscous damping eventually determines how aggressive the wind turbine controller can be tuned. Thus, the viscous drag and the blade pitch controller gains are obtained iteratively.

The parameterized control design routine has proven to be valid throughout the entire design space of platforms, which was verified through simulations over all operating wind speeds. Especially the rotor speed and power overshoots are for all platforms within the design space and the metocean conditions of [54, Chap. 7] inside commonly used design constraints.

4. Simulation Model

The numerical FOWT model used for the computation of the load response in this work was described in [43, 42]. Figure 4 shows a mechanical sketch of the Simplified Low-Order Wind Turbine (SLOW) model. The intended purpose of the model is to represent the overall rigid-body and elastic dynamics of the system. It shall, on the other side, disregard all effects which increase complexity without contributing to the main system response. Through the improvement of computational speed, an efficient calculation of the load response for all designs is possible. The model derivation starts with physical (as opposed to black-box) models, keeping the inherent nonlinearities. Subsequently, these models are linearized and the frequency-domain response spectra will be used here, which is subject of Section 5.

The structural model is derived using the theory of flexible MBS. An advantage of the implemented algorithm is that the setup of the equations of motion is user-defined. Thus, the multibody structure can be adapted to the analyzed problem. In this work, the equations of motion have been set up for six DoFs in 2D: The floating platform rigid body in surge (x_p), heave (z_p) and pitch (β_p), a flexible tower with one generalized coordinate x_t , the rotor speed Ω and the blade pitch actuator θ_1 is selected, see Figure 4. These DoFs are chosen with the aim of reducing the system to the most important forces and response dynamics. The largest environmental forces act usually in the direction of wind and waves (x).

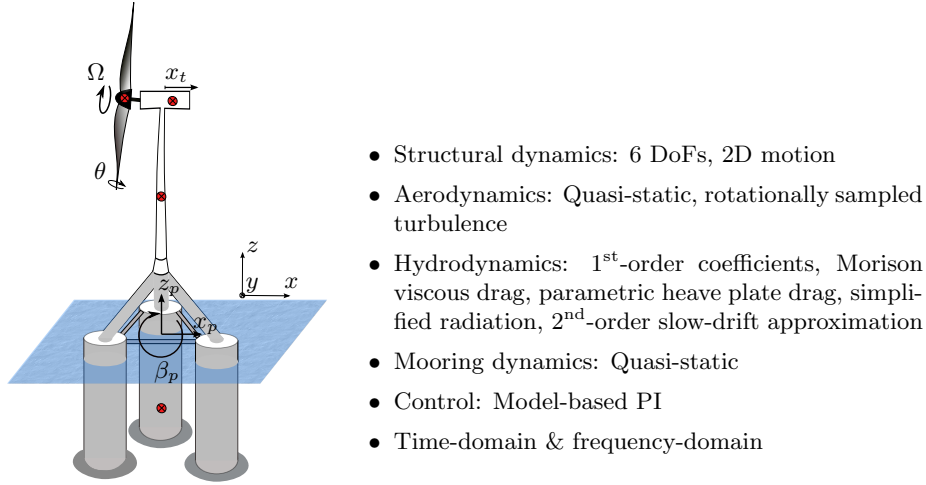


Figure 4: Low-order simulation model SLOW properties. Reprinted from [52] with permission from MDPI, 2018.

The aerodynamic model avoids an iterative solution of the lift and drag forces on the blade sections [55]. Instead, the bulk flow across the entire rotor is considered and the rotor thrust and torque is calculated as function of the Tip Speed Ratio (TSR) and the blade pitch angle, using the rotor thrust and power coefficient. This method neglects azimuth-dependent forcing, especially through wind shears. These are re-introduced through a rotational sampling of turbulence at the rotor rotational frequency. The method has proven to be a good tradeoff between accuracy and efficiency, especially for the optimization of the FOWT substructure, as shown in [43].

The hydrodynamic model uses the first-order panel code coefficients and a node-based Morison drag model for a reliable representation of the fore-aft viscous damping, as introduced in Section 1. A significant improvement of the computational efficiency is achieved through the frequency-independent added mass and the neglected radiation damping. It is shown in [43] that radiation damping is of little influence for the considered platforms, because the dominant forces at the frequencies of nonzero radiation damping are the first-order wave forces. Newman’s approximation [56] is employed to account for low-frequency slow-drift forcing. The mooring forces result from a quasi-static model.

The nonlinear equations of motion are linearized about all operating points, resulting in a linear state-space description. The aerodynamics are linearized with a tangent approximation of the rotor coefficients through a central difference scheme. The quadratic drag is linearized through Borgman’s method [57], using the Standard Deviation (STD) of the platform nodes, obtained from an iterative frequency-domain solution. The linear model is only valid for small

deviations of the states from the operating point. For this reason, the analyzed results focus on operational rather than extreme load cases. To prove the validity of the results, Section 5 will include a comparison against the higher-fidelity FAST model.

5. Load Calculation

This section presents the results of load calculations in operational conditions across the design space. First, selected signal statistics will be compared, weighted with the probability of occurrence of each environmental condition over a lifetime of 20 years in the same way as [58]. Thereafter, the frequency-domain response will be analyzed and the results will be verified through a comparison against the reference model FAST. A design indicator will be presented at the end of this section, which is able to predict the optimal response behavior.

The environmental conditions of the project LIFES50+ are used with a significant wave height up to $H_s = 8.3$ m, see Table 4. For each wind speed, three different peak spectral periods T_p are considered, each with a probability of occurrence of 1/3 for the respective mean wind speed. One-hour simulations are performed with both time-domain models, cutting the transient for statistical evaluation.

Table 4: Environmental conditions for operational load cases of [54, Chap. 7].

Wind speed \bar{v} [m/s]	5.0	7.1	10.3	13.9	17.9	22.1	25
Significant wave height H_s [m]	1.4	1.7	2.2	3.0	4.3	6.2	8.3
Peak spectral period T_{p1} [s]	5.0	5.0	5.0	7.0	7.5	10.0	10.0
T_{p2} [s]	7.0	8.0	8.0	9.5	10.0	12.5	12.0
T_{p3} [s]	11.0	11.0	11.0	12.0	13.0	15.0	14.0
Probability f [%]	14.8	25.0	28.7	17.5	5.9	0.9	0.1

5.1. Operational load response

The linear frequency-domain SLOW model of Section 4 is used to simulate the response to the metocean conditions of Table 4 for thirty platform designs of the parameter space of Figure 3.

Figure 5 shows the statistical results of the IEC Design Load Case (DLC) 1.2 [59], weighted with the Weibull probability density function of Table 4. The Damage-Equivalent Load (DEL) of the tower-base fore-aft bending moment M_{yt} is calculated for a lifetime of 20 years with a Wöhler exponent of $m = 4$. The STDs are normalized with the corresponding values for the onshore DTU 10 MW RWT with the same turbulent wind fields. For onshore turbines, the significant loading through the waves is not present and only the harmonic loads of the Once-Per-Revolution (1p) and 3p-frequencies are the main fatigue drivers. It can be seen that the weighted DEL of M_{yt} has a minimum at

the shallow-draft shape ($d = 24$ m, $h_{hp} = 4.5$ m). The same holds for the weighted STD of the rotor speed Ω (which is proportional to the power for above-rated winds) and the platform pitch angle β_p (here the minimum is at the thinnest heave plate $h_{hp} = 1.0$ m). The blade pitch activity (θ) is rather constant over the design space.

These results show a tower-base bending damage variation of more than 30 %. The fatigue damage is for the optimal design only 50 % greater than for the on-shore turbine, although the wave conditions are rather severe. The estimated material cost of this design is not significantly higher than the one of the deeper draft, see Figure 3, although the shallow-draft platform has a large column spacing of $d = 24$ m and a column radius of $r = 10.8$ m with heave plates of $r_{hp} = 17.4$ m.

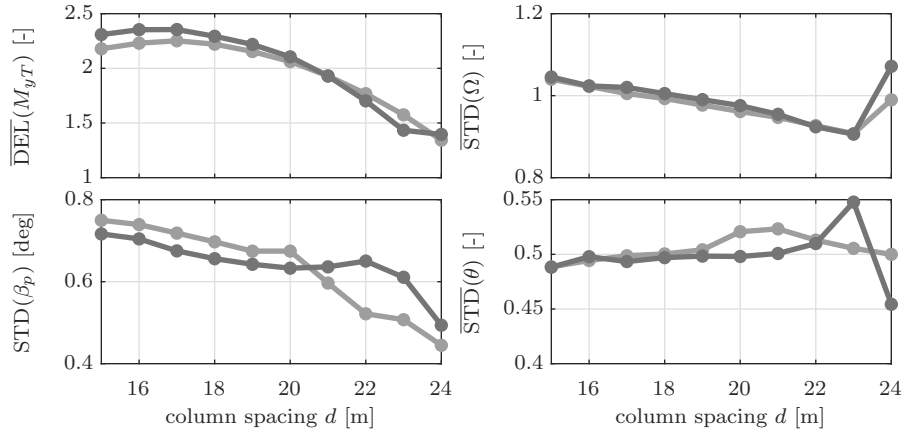


Figure 5: Linear response statistics of operational DLC1.2, of [54, Chap. 7], weighted according to wind speed distribution. $\overline{\text{DEL}}/\overline{\text{STD}}$ are normalized results with corresponding FAST onshore simulations of DTU 10 MW RWT with the same wind fields. Heave plate height $h_{hp} = [1.0, 8.0]$ m (increasing darkness), [43].

Figure 6 shows a comparison of the response spectra of the deep-draft and the shallow-draft platforms. The shallow-draft shape has a larger difference-frequency and wind-induced response in surge at the lower end of the frequency axis. Except for this, the reason for the good performance, indicated by Figure 5, becomes clear: The shallow-draft platform has visibly smaller responses at the pitch eigenfrequency of $f_{d,pitch} \approx 0.04$ Hz but, even more importantly, at the first-order wave frequencies of 0.1 Hz ($\bar{v}_{hub} = 17.9$ m/s, left) and 0.08 Hz ($\bar{v}_{hub} = 25$ m/s, right). This effect is noticeable for the platform motion response β_p but even more for the tower bending (x_t , M_{yt}), the rotor speed Ω and the electrical power P .

5.2. Comparison of design model and reference model

Figure 7 shows the same response signals as Figure 5 with a comparison between the nonlinear and the linearized SLOW models and the FAST model.

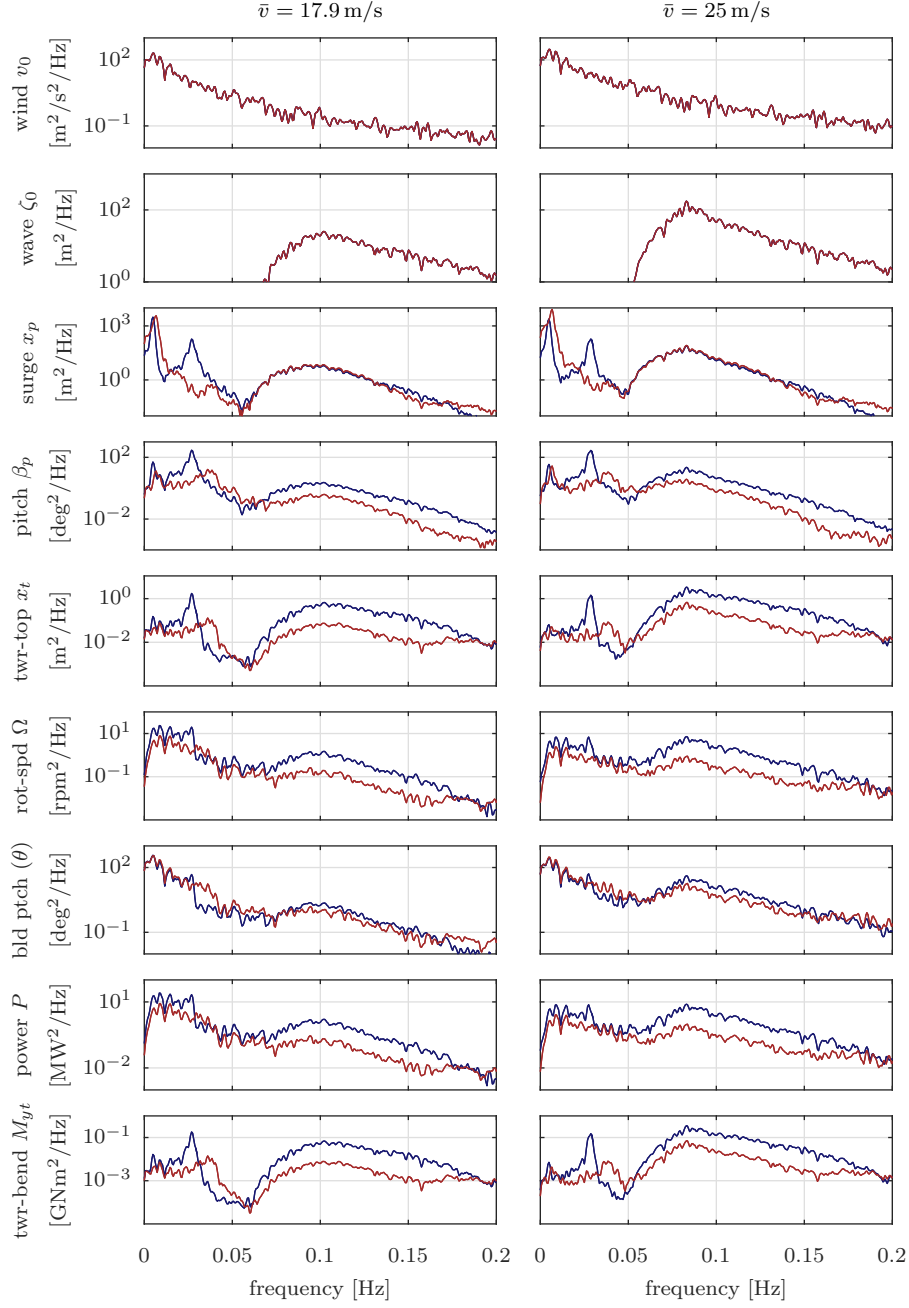


Figure 6: Comparison of deep-draft (spacing $d = 15$ m, blue) and shallow-draft (spacing $d = 24$ m, red) platforms for $\bar{v}_{hub} = 17.9$ m/s (left) and $\bar{v}_{hub} = 25.0$ m/s (right) with PI-controller, computed by FAST, [43].

The comparison shows the results of all column spacings d for the flattest heave plate $h_{hp} = 1.5$ m and the thickest heave plate $h_{hp} = 8$ m. The qualitative optimum towards large d (shallow drafts) is predicted equally by all models. Consequently, the low-order model is generally suitable for the considered conditions and assessed response quantities.

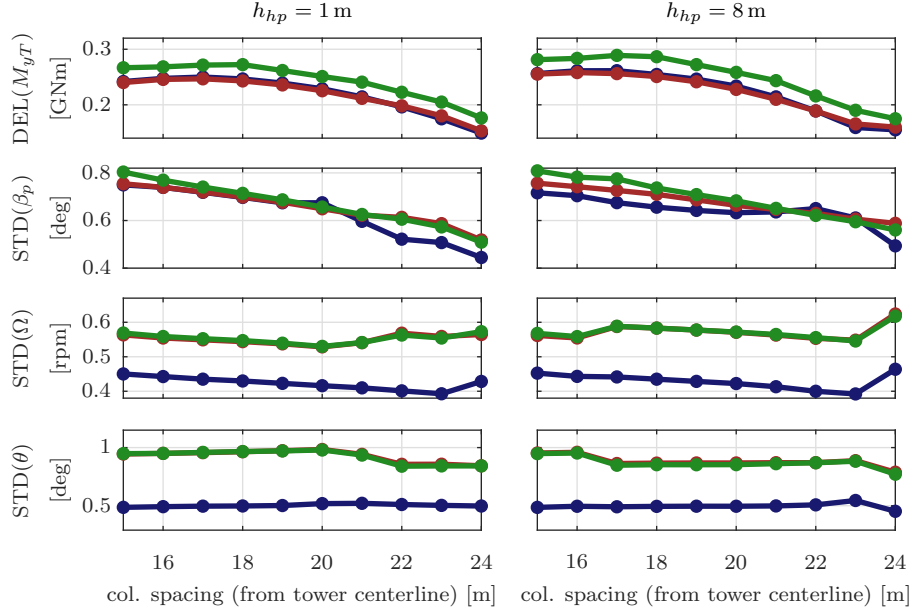


Figure 7: Response statistics of operational DLC1.2 with PI-controller, weighted for all wind speeds with distribution. Linear SLOW model (blue), nonlinear SLOW model (red), FAST (green), [43].

There is a constant concept-independent offset of the DEL between the SLOW models and FAST. The reason for this offset is the simplified actuator disk model. The excitation of the blades through wind shear is only reintroduced through a rotational sampling of the blade-effective wind at the nominal rotor speed, see [42]. The offset of the rotor speed Ω and blade pitch angle θ is related to the linearized SLOW model. The linearized model underpredicts the variation of the rotor responses because of the nonlinear switching algorithm of the controller. The objective of the below-rated controller is to maximize power production, while the above-rated controller aims at limiting the power production. The switching between the control regions is a highly nonlinear effect, which cannot be modeled with the linear frequency-domain model. It is, however, modeled in the time-domain model, which agrees notably better with FAST for Ω and θ . The platform pitch angle variation is well aligned among the time-domain models with a slight underprediction of SLOW for the platforms of deep draft. The linearized model underpredicts the pitch-STD for the shallow-draft platforms. This effect is distinct for the two heave plate heights h_{hp} and might therefore be due to the simplified radiation model,

see [42].

5.3. Extreme load response

The load response to IEC DLC 6.1 with 50-year wind and wave conditions is presented in this section. The reference model FAST was used in this case because of large expected excursions, where especially the aerodynamic model of SLOW might not predict reliable results, due to its simplifications. Turbulent wind and irregular wave timeseries were generated according to [54, p. 58, 64]. Figure 8 shows the mean of the maxima of the tower-base bending moment M_{yt} and the tower-top acceleration \ddot{x}_{tt} (the absolute one, including platform accelerations) of three one-hour simulations. The results confirm the findings of Figure 5: The shallow-draft platform has small tower-top accelerations of less than $0.3g$. The LIFES50+ design basis [60] would accept these values even during operation, while the limits for shut-down conditions are $\ddot{x}_{tt,max} = 0.3g$.

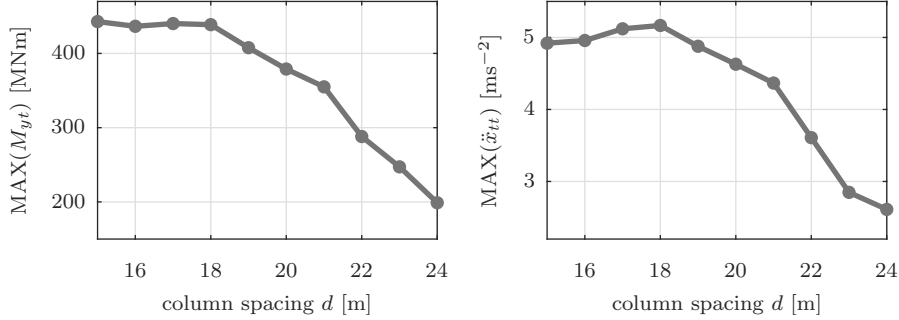


Figure 8: DLC 6.1 extreme sea state with 50-year extreme conditions of $\bar{v}_{50} = 44$ m/s, $H_s = 10.9$ m and $T_p = 15$ s. Tower-base bending moment (left) and absolute tower-top acceleration (right) simulated with FAST. Heave plate height $h_{hp} = 4.5$ m.

6. Results Analysis and Design Indicators

A key to understanding the underlying effect for this remarkable ability of the shallow-draft platform ($d = 24$ m) to reject disturbances is the analysis how the system responds to sinusoidal disturbances, meaning regular waves of different frequencies or harmonically oscillating wind speed. The ability to reject these disturbances will be quantified with a new design indicator at the end of this section.

6.1. Harmonic response to wind and waves

Figure 9 shows the harmonic response to wind and wave forces. The lines, representing each a different frequency, stand for the FOWT centerline response. The horizontal distance of each point on the lines to the y -axis indicates the amplitude of oscillation of the system response at all elevations z along the centerline to sinusoidal wind (upper) and wave excitations (lower). The analysis is

made with the low-order linearized model of Section 4 with first-order hydrodynamics, quasi-static mooring lines, an elastic tower, aerodynamics and the tuned PI-controller at $\bar{v}_{hub} = 13.9 \text{ m/s}$. The centerline amplitude $|\Phi_{x,i}(z, \omega)|$ results from the disturbance transfer function or Response Amplitude Operator (RAO) $G_{di,x_k}(\omega)$ from wind ($i = 1$) and waves ($i = 2$) to the states surge, pitch and tower-bending, represented by x_k as

$$|\Phi_{x,i}(z, \omega)| = |G_{di,x_p}(\omega) + G_{di,\beta_p}(\omega)z + G_{di,x_t}(\omega)\varphi_x(z)|. \quad (3)$$

The tower shape function is denoted by $\varphi_x(z)$.

The solid black horizontal lines indicate the overall Center of Mass (CM) of the FOWT and the dashed line indicates the center of buoyancy. For ships, the instantaneous center of roll motions is usually the metacenter, [61, p. 62]. Here, the instantaneous center of rotation in pitch is the vertical location on the platform with near-zero amplitude. The response to harmonic wind excitations shows a center of rotation equal to the CM. The same behavior is generally observable for all platforms.

The lower part of Figure 9 shows the harmonic response to waves. Here, the instantaneous center of rotation is below the platform-CM for the platforms of deep draft. The platform of the lowest draft ($d = 24 \text{ m}$) has a different behavior: Its instantaneous center of rotation is at higher elevations, near the rotor hub. This is remarkable because it means that the hub does not respond with a horizontal movement to wave excitations. Consequently, the wind turbine power production is almost not affected by the waves and the rotor does not see any platform-induced relative wind speed. The shallow-draft platform responds in a way that surge is positive, when pitch is negative. Thus, these DoFs are out-of-phase, as opposed to the other platforms, which have an in-phase response of surge and pitch to waves. Therefore, this optimality cannot be found when the surge or pitch RAO is sought to be minimized. The same idea inspired the developers of a TLP platform to arrange the taut mooring lines, such that the system is forced to rotate about the hub, see [62]. The fact that this behavior can be obtained for semi-submersibles has not been published yet.

The cause leading to this response behavior are the Froude-Krylov pressures, integrated over the hull surface. The coupled magnitude and phases of the force-RAO vector $\mathbf{X}(\omega)$ are for the optimal shape such that the presented response of the FOWT system is obtained. Semi-submersibles are predestined for a “shaping” of the force-RAO because the floater members see different phases of the waves and, additionally, the horizontal (heave plates) and vertical (columns) surfaces experience different phases of the Froude-Krylov pressures, which allow a counter-phase surge and pitch forcing.

Eventually, the shallow-draft platform motion is not constrained but a motion response to mitigate the wave pressures is allowed. Important is the fact that the allowed motion response is favorable, such that the transmissibility of the wave forcing towards the wind turbine is reduced. The smaller tower-top motion yields smaller inertial forces of the Rotor-Nacelle Assembly (RNA). The bending moments from the gravitational forces of the RNA are reduced because

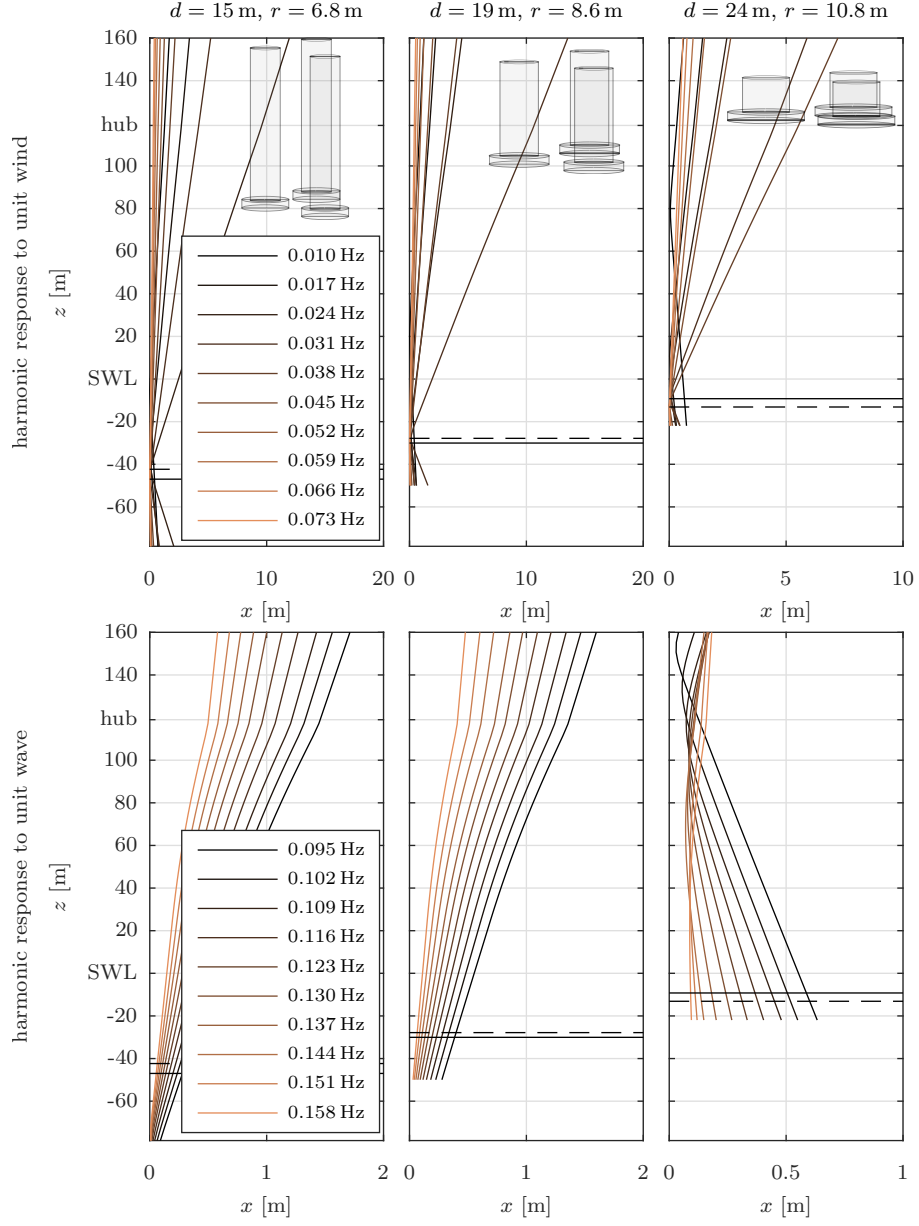


Figure 9: Harmonic response of FOWT system over typical wind frequencies (top) and wave frequencies (bottom) at $v_0 = 13.9$ m/s with heave plate height $h_{hp} = 4.5$ m. Solid black line: FOWT overall center of mass, dashed black line: center of buoyancy, [43].

the platform pitch angle is also smaller for the shallow-draft design (Figure 5). The aerodynamic damping forces are not significant at the wave frequencies [63]. In conclusion, the stationary hub does not only yield a smooth power production but also reduced tower-base bending moments. Small adjustments in the optimal harmonic response shape can be expected when taking other outputs, like the mooring fatigue, into account.

The “counter-phase pitch response” of Figure 9 is important for the controller design: Because of the minimal motion response at the hub, the power fluctuations are reduced. Also, the coupling of the substructure dynamics with the controller is reduced. Common controllers feed back the rotor speed deviation from the set point. If the rotor responds less to the wave forces, there will be less wave-induced rotor speed deviation and the wave response will not be amplified by the controller as with regular FOWT platforms. It is emphasized that the harmonic response is not to be confused with the modal response to turbulence and slow-drift forces. This one can be well damped by wind turbine controllers, which feed back a fore-aft velocity signal, as in [64], [65] or [66]. It was shown in [64, 63] that the system response to first-order waves cannot be damped by the controller because of their large magnitude. Consequently, the shaping of the hull which yields the favorable first-order wave response can be effectively complemented by a controller, which damps the low-frequency motion response.

The sensitivity of this behavior to the peak spectral wave period T_p is obvious from Figure 9. Thus, the favorable design is site-dependent. It can be seen, however, that the sensitivity is not very pronounced, meaning that the instantaneous center of rotation does not move significantly as a function of the wave frequency. This shows a certain robustness of the response behavior in terms of the environmental conditions.

6.2. Design indicator: Minimum required control action

The harmonic response of Figure 9 helps to understand the reason for the favorable behavior of the shallow-draft platforms. In this section, a new design indicator will be introduced to generally judge the goodness of a platform in terms of its induced wind turbine response. The idea is to quantify the necessary controller action to perfectly cancel the external forcing from wind and waves. The smaller the controller activity, the better the capability of the design to inherently reject disturbances itself. Figure 10 shows the linear FOWT system transfer function in the Laplace domain $\mathbf{G}(j\omega)$ with additive disturbance transfer functions $\mathbf{G}_{d,i}$ for the control inputs generator torque and blade pitch angle $\mathbf{u} = [M_g, \theta]^T$ and the outputs rotor speed and tower-top bending $\mathbf{y} = [\Omega, x_t]^T$. Both, the plant $\mathbf{G}(j\omega)$ and the disturbance transfer function for wind $G_{d,v_0}(j\omega)$ and the one for waves $G_{d,\zeta}(j\omega)$, collected in \mathbf{G}_d , are obtained from the linear SLOW model and scaled as in [63]. This is convenient as it means that a response $y_i \geq 1$ exceeds the design limits, see [67].

In order to quantify the impact of disturbances on a linear system, Skogestad [68] calculates the 2-norm of the control input, theoretically necessary

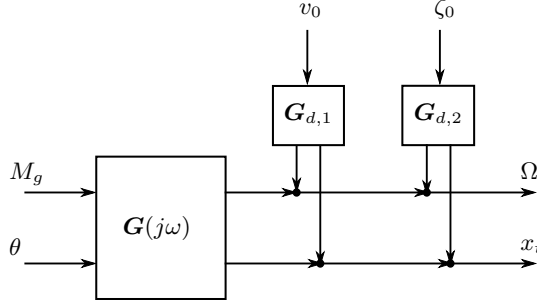


Figure 10: FOWT square plant with additive disturbances.

to perfectly cancel the disturbances. This analysis does not consider the controller dynamics but only the actuator authority on the system response. The required control input \mathbf{u} can be obtained, given a disturbance \mathbf{d} , through system inversion as

$$\mathbf{u} = -\mathbf{G}^{-1}(j\omega)\mathbf{G}_d(j\omega)\mathbf{d}. \quad (4)$$

The least necessary actuation⁴ has been calculated for the different platforms for the wind excitation $d = v_0 = 1$ and wave excitation $d = \zeta_0 = 1$ independently in Figure 11. The part from wind excitation (upper part of Figure 11) does not show a large variation over the different platforms, except for the changing eigenfrequencies. It is different for the wave excitation: The best performance (equal to the least required actuation U_{min}^*) results here for the largest column spacing $d = 24$ m. Consequently, the assessment of the minimum required control input can well predict the optimality of the semi-submersibles, seen in the Figure 5 and 9.

This indicator allows a general quantification of the ability of a FOWT platform to support a wind turbine without transmitting detrimental external excitation forces. It is the basis for a platform design, particularly adapted to the requirements of the wind turbine.

Parameters of optimum design. A FAST model of the optimum shape can be downloaded [69]. The hull shape has a column radius of $r = 10.81$ m, a spacing from the centerline of $d = 24$ m a heave plate thickness of $h_{hp} = 4.5$ m a draft of $t = 21.94$ m. The platform has a mass including ballast of $m = 3.115 \times 10^4$ t and a center of mass below SWL of $z_{cm,ptfm} = 13.36$ m.

7. Conclusions

The study can be summarized by two parts:

⁴Calculated for both control inputs \mathbf{u} , assuming the most effective combination of them, through a Singular Value Decomposition (SVD) of \mathbf{G} . $U_{min}^*(\omega)$ is the 2-norm of the control input vector.

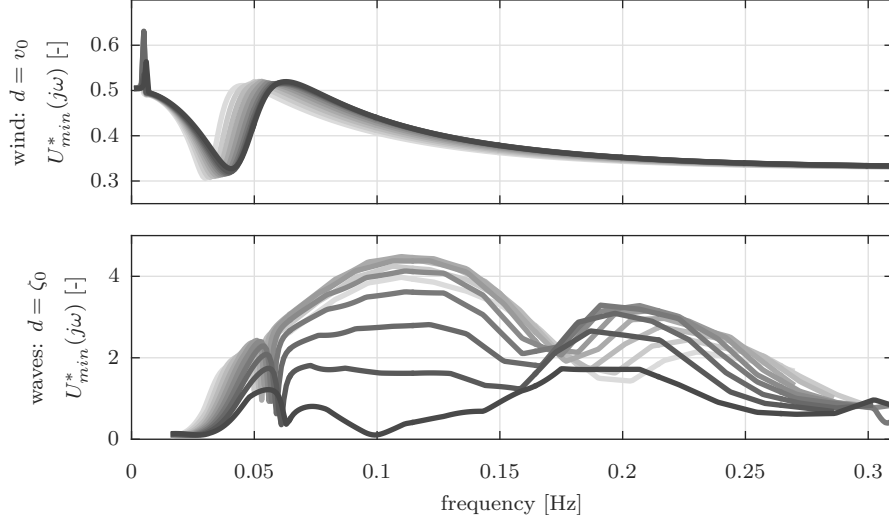


Figure 11: Minimum required control input magnitude U_{min}^* to perfectly reject wind (top) and wave (bottom) disturbances assuming the strongest combination of control inputs $\mathbf{u} = [M_g, \theta]$ for platforms of different column spacings $d = [15(1)24]$ m (increasing darkness) and $h_{hp} = 4.5$ m, [43].

First, an integrated optimization procedure for semi-submersible FOWTs was set up. A small design space of a three-column semi-submersible with heave plates was defined, ranging from a slender deep-drafted geometry to a shallow-draft one with large column diameter. A tailored coupled simulation model of low order was employed to calculate the system response, but also for the design of a wind turbine controller that is tuned for each platform design. As a result of the optimization, the design of lower draft gave a remarkable improvement of the response of the tower-base bending.

Second, a detailed analysis of the results revealed a particularly favorable response behavior to first-order waves, which can be represented by a new design indicator. The identified optimum is mainly due to an efficient design of the hull shape, yielding a favorable response behavior: The harmonic response function, derived from a linearized low-order model, revealed the dynamic characteristics of the optimum shape. It shows almost no fore-aft motion at the rotor hub, which means that the entire system, subject to wave loads, rotates about this point. As a result, the hub is almost stationary and the fluctuations of the power, the rotor speed, generator torque and blade pitch angle can be significantly reduced. An interpretation of this is that the surge and pitch response are out-of-phase, yielding a positive surge displacement when the pitch angle is negative.

In order to consider this optimal dynamic behavior of semi-submersibles in future design practices, a new performance indicator was developed: The “least required actuator action” is considered, the action of the blade pitch angle and

generator torque. Their magnitude, necessary to reject the wave loads, is an indicator, which can effectively predict how well a floating platform is able to inherently reject disturbances itself, without transmitting them to the wind turbine.

The study showed that it is possible to design a FOWT platform, specifically suitable to carry a wind turbine, minimizing the effect of the waves on the power production. While the first-order wave loads cannot be mitigated by the controller, a further improvement of the low-frequency response behavior through the controller is possible. The presented harmonic response graph can be a good means for the selection of additional feedback loops. Although the cost model of this work is simple, the work follows the idea that a smooth behavior in harsh met-ocean conditions is a key for a sustainable and low-cost FOWT design.

Further studies will address the impact of the counter-phase response on the mooring line loads and integrate them into an optimization process.

Acknowledgements

The research leading to these results has received funding from the European Union's Horizon 2020 research and innovation programme under grant agreement No. 640741 (LIFES50+).

References

- [1] A. Henderson, Analysis tools for large floating offshore wind farms, Ph.D. thesis, University College London (2000).
- [2] J. O. G. Tande, K. Merz, U. S. Paulsen, H. G. Svendsen, Floating offshore turbines, *Wiley Interdisciplinary Reviews: Energy and Environment* 4 (3) (2015) 213–228. doi:10.1002/wene.130.
- [3] NWTC, NWTC information portal (FAST v8) (2016).
URL <https://nwtc.nrel.gov/FAST8>
- [4] J. Jonkman, Influence of control on the pitch damping of a floating wind turbine, in: *Proceedings of the 46th AIAA Aerospace Sciences Meeting and Exhibit*, AIAA, Reno, USA, 2008. doi:10.2514/6.2008-1306.
- [5] T. J. Larsen, T. D. Hanson, A method to avoid negative damped low frequent tower vibrations for a floating, pitch controlled wind turbine, *Journal of Physics: Conference Series* 75. doi:10.1088/1742-6596/75/1/012073.
- [6] M. O. L. Hansen, Influence of rigid body motions on rotor induced velocities and aerodynamic loads of a floating horizontal axis wind turbine, in: *Proceedings of the ASME 33rd International Conference on Ocean, Offshore and Arctic Engineering*, San Francisco, USA, 2014. doi:10.1115/OMAE2014-24227.

- [7] T. T. Tran, D. H. Kim, The platform pitching motion of floating offshore wind turbine: A preliminary unsteady aerodynamic analysis, *Journal of Wind Engineering and Industrial Aerodynamics* 142 (2015) 65–81. doi:10.1016/j.jweia.2015.03.009.
- [8] M. Lennie, D. Marten, G. Pechlivanoglou, C. N. Nayeri, C. O. Paschereit, Modern methods for investigating the stability of a pitching floating platform wind turbine, *Wind Energy Science* 2 (2) (2017) 671–683. doi:10.5194/wes-2-671-2017.
- [9] D. Matha, F. Lemmer, M. Muskulus, Offshore turbines with bottom-fixed or floating substructures, in: P. Veers (Ed.), *Wind Energy Modeling and Simulation - Volume 2: Turbine and System*, The IET, 2019. doi:10.1049/PBP0125G_ch5.
- [10] J. Journée, W. W. Massie, *Offshore Hydromechanics*, 1st Edition, Delft University of Technology, 2001.
URL https://ocw.tudelft.nl/wp-content/uploads/OffshoreHydromechanics_Journee_Massie.pdf
- [11] M. E. McCormick, *Ocean Engineering Mechanics*, Cambridge University Press, New York, 2010.
- [12] O. M. Faltinsen, *Sea Loads On Ships And Offshore Structures*, Cambridge University Press, 1993.
- [13] T. Duarte, A. Sarmento, J. Jonkman, Effects of second-order hydrodynamic forces on floating offshore wind turbines, in: *Proceedings of the AIAA SciTech*, National Harbor, USA, 2014. doi:10.2514/6.2014-0361.
- [14] S. Y. Hanna, Wave cancellation effects and extreme wave dynamics, in: *Proceedings of the Offshore Technology Conference*, Houston, USA, 1986.
- [15] M. H. Patel, *Dynamics of offshore structures*, 1st Edition, Butterworths, London, 1989.
- [16] J. Azcona, D. Palacio, X. Munduate, L. González, T. A. Nygaard, Impact of mooring lines dynamics on the fatigue and ultimate loads of three offshore floating wind turbines computed with IEC 61400-3 guideline, *Wind Energy* 20 (5) (2016) 797–813. arXiv:arXiv:1006.4405v1, doi:10.1002/we.2064.
- [17] D. Matha, Impact of aerodynamics and mooring system on dynamic response of floating wind turbines, Ph.D. thesis, University of Stuttgart (2016).
- [18] F. Huijs, J. Mikx, F. Savenije, E.-J. D. Ridder, Integrated design of floater, mooring and control system for a semi-submersible floating wind turbine, in: *Proceedings of the European Wind Energy Association Offshore Wind Conference and Exhibition*, 2013.

- [19] J. Azcona, D. Bekiropoulos, H. Bredmose, A. Fischer, N. F. Heilskov, A. Krieger, T. Lutz, A. Manjock, D. Manolas, D. Matha, K. Meister, R. Pereira, J. Ronby, F. Sandner, S. Voutsinas, INNWIND.EU D4.21: State-of-the-art and implementation of design tools for floating structures, Tech. Rep. November, INNWIND.EU (2013).
- [20] J. Fernandez, A. Laidler, J. Izarra, M. Innovation, D. Murueta, B. Malloape, Design considerations of a semisubmersible platform for offshore wind turbines, in: Proceedings of the European Wind Energy Association Offshore Wind Conference and Exhibition, 2013.
- [21] A. Crozier, Design and dynamic modeling of the support structure for a 10MW offshore wind turbine (2011).
- [22] J. Liu, E. Thomas, L. Manuel, D. Griffith, K. Ruehl, M. Barone, Integrated system design for a large wind turbine supported on a moored semi-submersible platform, Journal of Marine Science and Engineering 6 (1) (2018) 9. doi:10.3390/jmse6010009.
- [23] K. Müller, F. Lemmer, F. Borisade, M. Kretschmer, J. Gruber, L. Hagemann, N.-D. Nguyen, L. Vita, LIFES50+ D7.4 State-of-the-art FOWT design practice and guidelines, Tech. rep., University of Stuttgart (2015). URL http://lifes50plus.eu/wp-content/uploads/2015/11/GA_640741_LIFES50_D7.4.pdf
- [24] M. Atcheson, A. Garrad, L. Cradden, A. Henderson, D. Matha, J. Nichols, D. Roddier, J. Sandberg, Floating Offshore Wind Energy, Springer, 2016.
- [25] S. Lefebvre, M. Collu, Preliminary design of a floating support structure for a 5MW offshore wind turbine, Ocean Engineering 40 (2012) 15–26. doi:10.1016/j.oceaneng.2011.12.009. URL <http://linkinghub.elsevier.com/retrieve/pii/S0029801811002769>
- [26] C. Molins, A. Campos, F. Sandner, D. Matha, Monolithic concrete offshore floating structure for wind turbines, in: Proceedings of the European Wind Energy Association Annual Event, Barcelona, Spain, 2014.
- [27] D. Matha, F. Sandner, C. Molins, A. Campos, P. W. Cheng, Efficient preliminary floating offshore wind turbine design and testing methodologies and application to a concrete spar design, Philosophical Transactions of the Royal Society A 373 (2035). doi:10.1098/rsta.2014.0350.
- [28] C. Molins, A. Yagüe, P. Trubat, Construction possibilities for monolithic concrete spar buoy serial production, Journal of Physics: Conference Series 1104 (2018) 012020. doi:10.1088/1742-6596/1104/1/012020.
- [29] S. de Guzmán, D. Marón, P. Bueno, M. Tabaoda, M. Moreu, A reduced draft spar concept for large offshore wind turbines, in: Proceedings of the

ASME 37th International Conference on Ocean, Offshore and Arctic Engineering, Madrid, Spain, 2018. doi:10.1115/OMAE2018-77787.

- [30] B. Pereyra, Z. Jiang, Z. Gao, M. T. Andersen, H. Stiesdal, Parametric study of a counter weight suspension system for the tetraspar floating wind turbine, in: Proceedings of the ASME 2018 1st International Offshore Wind Technical Conference, ASME, San Francisco, USA, 2018.
- [31] A. Aubault, C. Cermelli, D. Roddier, Windfloat: A floating foundation for offshore wind turbines part III: Structural analysis, in: Proceedings of the ASME 28th International Conference on Ocean, Offshore and Arctic Engineering, 2009. doi:10.1115/OMAE2009-79232.
- [32] C. Luan, Z. Gao, T. Moan, Modelling and analysis of a semi-submersible wind turbine with a central tower with emphasis on the brace system, in: Proceedings of the ASME 32nd International Conference on Ocean, Offshore and Arctic Engineering, ASME, Nantes, France, 2013. doi:10.1115/OMAE2013-10408.
- [33] C. Luan, Z. Gao, T. Moan, Development and verification of a time-domain approach for determining forces and moments in structural components of floaters with an application to floating wind turbines, *Marine Structures* 51 (2017) 87–109. doi:10.1016/j.marstruc.2016.10.002.
- [34] M. Borg, H. Bredmose, A. M. Hansen, Elastic deformations of floaters for offshore wind turbines: dynamic modelling and sectional load calculations, in: Proceedings of the ASME 36th International Conference on Ocean, Offshore and Arctic Engineering, Trondheim, Norway, 2017. doi:10.1115/OMAE2017-61466.
- [35] T. A. Nygaard, Design, analysis and wave tank testing of a semi-submersible braceless concrete offshore wind turbine platform, in: EERA Deepwind, Trondheim, Norway, 2015.
URL http://www.sintef.no/Projectweb/Deepwind_2015/Presentations/
- [36] P. D. Sclavounos, C. Tracy, S. Lee, Floating offshore wind turbines: Responses in a seastate, pareto optimal designs and economic assessment, in: Proceedings of the ASME 27th International Conference on Offshore Mechanics and Arctic Engineering, 2007. doi:10.1115/OMAE2008-57056.
- [37] I. Fylling, P. A. Berthelsen, Windopt – An optimization tool for floating support structures for deep water wind turbines, in: Proceedings of the ASME 30th International Conference on Ocean, Offshore and Arctic Engineering, ASME, Rotterdam, Netherlands, 2011. doi:10.1115/OMAE2011-49985.

- [38] F. Sandner, D. Schlipf, D. Matha, P. W. Cheng, Integrated optimization of floating wind turbine systems, in: Proceedings of the ASME 33rd International Conference on Ocean, Offshore and Arctic Engineering, San Francisco, USA, 2014. doi:10.1115/OMAE2014-24244.
- [39] F. Lemmer, K. Müller, W. Yu, D. Schlipf, P. W. Cheng, Optimization of floating offshore wind turbine platforms with a self-tuning controller, in: Proceedings of the ASME 36th International Conference on Ocean, Offshore and Arctic Engineering, Trondheim, Norway, 2017. doi:10.1115/OMAE2017-62038.
- [40] M. Hall, B. Buckham, C. Crawford, Evolving offshore wind: A genetic algorithm-based support structure optimization framework for floating wind turbines, in: Proceedings of the OCEANS MTS/IEEE, IEEE, Bergen, Norway, 2013. doi:10.1109/OCEANS-Bergen.2013.6608173.
- [41] M. Karimi, Frequency Domain Modeling and Multidisciplinary Design Optimization of Floating Offshore Wind Turbines, Ph.D. thesis, University of Victoria, Canada (2018).
URL https://www.researchgate.net/publication/328575575_Frequency_domain_modeling_and_multidisciplinary_design_optimization_of_floating_offshore_wind_turbines
- [42] F. Lemmer, W. Yu, B. Luhmann, D. Schlipf, P. W. Cheng, Multibody modeling for concept-level floating offshore wind turbine design, Multibody System Dynamics 49 (2) (2020) 203–236. doi:10.1007/s11044-020-09729-x.
- [43] F. Lemmer, Low-Order Modeling, Controller Design and Optimization of Floating Offshore Wind Turbines, Ph.D. thesis, University of Stuttgart (2018).
- [44] C. Bak, F. Zahle, R. Bitsche, T. Kim, A. Yde, L. Henriksen, M. H. Hansen, J. Blasques, M. Gaunaa, A. Natarajan, The DTU 10-MW Reference Wind Turbine, Tech. rep., Technical University of Denmark, Roskilde, Denmark (2013).
URL <https://orbit.dtu.dk/en/publications/the-dtu-10-mw-reference-wind-turbine>
- [45] F. Lemmer, K. Müller, A. Pegalajar-Jurado, M. Borg, H. Bredmose, LIFES50+ D4.1: Simple numerical models for upscaled design, Tech. rep., University of Stuttgart (2016).
URL https://lifes50plus.eu/wp-content/uploads/2018/04/LIFES50_D4-1_final_rev1_public.pdf
- [46] F. Sandner, W. Yu, D. Matha, J. Azcona, X. Munduate, E. Grela, S. Voutsinas, A. Natarajan, INNWIND.EU D4.33: Innovative concepts for floating structures, Tech. rep., University of Stuttgart (2014).
URL <http://www.innwind.eu/-/media/Sites/innwind/>

- [47] H. Bredmose, F. Lemmer, M. Borg, A. Pegalajar-Jurado, R. F. Mikkelsen, T. Stoklund Larsen, T. Fjelstrup, W. Yu, A. K. Lomholt, L. Boehm, J. Azcona, The TripleSpar campaign: Model tests of a 10MW floating wind turbine with waves, wind and pitch control, *Energy Procedia* 137 (2017) 58–76. doi:10.1016/j.egypro.2017.10.334.
- [48] G. Benveniste, M. Lerch, M. de Prada, M. Kretschmer, J. Berque, A. López, G. Pérez-Morán, LIFES50+ D2.2 LCOE tool description, technical and environmental impact evaluation procedure, Tech. rep., Catalonia Institute for Energy Research, Barcelona, Spain (2015).
URL http://lifes50plus.eu/wp-content/uploads/2016/10/GA_640741_D2.2-internal.pdf
- [49] M. Lerch, M. De-Prada-Gil, C. Molins, G. Benveniste, Sensitivity analysis on the levelized cost of energy for floating offshore wind farms, *Sustainable Energy Technologies and Assessments* 30 (2018) 77–90. doi:10.1016/j.seta.2018.09.005.
- [50] F. Lemmer, K. Müller, W. Yu, R. Faerron-Guzmán, M. Kretschmer, LIFES50+ D4.3 Optimization framework and methodology for optimized floater design, Tech. rep., University of Stuttgart (2016).
URL http://lifes50plus.eu/wp-content/uploads/2015/11/GA_640741_LIFES50_D4.3-web.pdf
- [51] L. Tao, D. Dray, Hydrodynamic performance of solid and porous heave plates, *Ocean Engineering* 35 (10) (2008) 1006–1014. doi:10.1016/j.oceaneng.2008.03.003.
- [52] F. Lemmer, W. Yu, P. W. Cheng, Iterative frequency-domain response of floating wind turbines with parametric drag, *Journal of Marine Science and Engineering* 6 (4). doi:10.3390/jmse6040118.
- [53] F. Lemmer, W. Yu, D. Schlipf, P. W. Cheng, Robust gain scheduling baseline controller for floating offshore wind turbines, *Wind Energy* 23 (1). doi:10.1002/we.2408.
- [54] A. Krieger, G. K. V. Ramachandran, L. Vita, P. Gómez Alonso, J. Berque, G. Aguirre-Suso, LIFES50+ D7.2 Design basis, Tech. rep., DNV-GL (2016).
URL http://lifes50plus.eu/wp-content/uploads/2015/11/D72_Design_Basis_Retyped-v1.1.pdf
- [55] M. O. L. Hansen, *Aerodynamics of Wind Turbines*, 2nd Edition, Earthscan, 2000.

- [56] R. Standing, W. Brendling, D. Wilson, Recent developments in the analysis of wave drift forces, low-frequency damping and response, in: Proceedings of the Offshore Technology Conference, Houston, USA, 1987. doi:10.4043/5456-MS.
- [57] L. E. Borgman, The spectral density for ocean wave forces, in: Proceedings of the Santa Barbara Coastal Engineering Conference, Santa Barbara, USA, 1965, pp. 147–182. arXiv:uuid:ad7a5c81-2a6e-45dc-868d-1cce4fd95df1.
- [58] E. Smilden, E. E. Bachynski, A. Sørensen, Key contributors to lifetime accumulated fatigue damage in an offshore wind turbine support structure, in: Proceedings of the ASME 36th International Conference on Ocean, Offshore and Arctic Engineering, Trondheim, Norway, 2017. doi:10.1115/OMAE2017-61708.
- [59] IEC, 61400-3 Wind turbines - Part 3: Design requirements for offshore wind turbines (2007).
- [60] G. Ramachandran, L. Vita, A. Krieger, K. Mueller, Design basis for the feasibility evaluation of four different floater designs, Energy Procedia 137 (2017) 186–195. doi:10.1016/j.egypro.2017.10.345.
- [61] T. Fossen, Handbook of Marine Craft Hydrodynamics and Motion Control, 1st Edition, John Wiley and Sons, 2011. doi:10.1002/9781119994138.
- [62] C. Melis, F. Caille, T. Perdrizet, Y. Poirrette, P. Bozonnet, A novel tension-leg application for floating offshore wind: Targeting lower nacelle motions, in: Proceedings of the ASME 35th International Conference on Ocean, Offshore and Arctic Engineering, Busan, South Korea, 2016. doi:10.1115/OMAE2016-54961.
- [63] F. Lemmer, D. Schlipf, P. W. Cheng, Control design methods for floating wind turbines for optimal disturbance rejection, Journal of Physics: Conference Series 753. doi:10.18419/opus-8906.
- [64] P. Fleming, A. Peiffer, D. Schlipf, Wind turbine controller to mitigate structural loads on a floating wind turbine platform, in: Proceedings of the ASME 35th International Conference on Ocean, Offshore and Arctic Engineering, Busan, Korea, 2016. doi:10.1115/OMAE2016-54536.
- [65] J. Olondriz, I. Elorza, C. Calleja, J. Jugo, A. Pujana, Platform negative damping, blade root and tower base bending moment reductions with an advanced control technique, in: Proceedings of the WindEurope Conference and Exhibition, Amsterdam, Netherlands, 2017.
- [66] W. Yu, F. Lemmer, D. Schlipf, P. W. Cheng, B. Visser, H. Links, N. Gupta, S. Dankelmann, B. Couñago, J. Serna, Evaluation of control methods for floating offshore wind turbines, Journal of Physics: Conference Series 1104 (2018) 012033. doi:10.1088/1742-6596/1104/1/012033.

- [67] S. Skogestad, I. Postlethwaite, Multivariable Feedback Control: Analysis and Design, 2nd Edition, John Wiley and Sons, Chichester, 2007.
- [68] S. Skogestad, E. Wolff, Controllability measures for disturbance rejection, *Journal of Modeling, Identification and Control* 17 (3) (1996) 167–182. doi:10.4173/mic.1996.3.1.
- [69] F. Lemmer, K. Müller, W. Yu, FAST model of the SWE-CPP semi-submersible floating wind turbine platform for the DTU 10MW reference wind turbine (2020). doi:10.18419/darus-621.